Initial Rotor Position Estimation Method for PM Motors

Marco Tursini, *Member, IEEE*, Roberto Petrella, *Member, IEEE*, and Francesco Parasiliti

***Abstract*—This paper presents a method to detect the rotor position of permanent-magnet motors at standstill, which is suitable to avoid temporary reverse rotation at startup or starting failure.**

The approach is based on the investigation of the stator inductance variation as a function of the rotor magnets position and the stator current space vector. It involves the application of a proper sequence of voltage pulses to the stator windings, and the measurement of the peak values of the resulting current in order to achieve the rotor position estimation. Actually, the current measurements show significant uncertainties which affect the rotor position detection. In order to avoid these problems, the authors propose a novel procedure which combines an iterative sequence of voltage pulses with a fuzzy logic processing of the current responses and phase currents derivation based on the dc-link current measurements.

The proposed method has been implemented on a μC digital signal processor (TMS320F240). The obtained results confirm the effectiveness of the proposed solution. It can be applied in sensorless drives, in drives equipped with nonabsolute position transducers, with a wide range of motors, and it does not require the knowledge of any of the motor parameters.

***Index Terms*—Fuzzy logic, permanent-magnet (PM) motor, rotor angle detection, voltage injection.**

NOMENCLATURE

$h \in \{A, B, C\}$	Index for phase labels.
$\hat{}$	Amplitude/normalized value.
$\tilde{a}, \Delta$	Estimate, difference/correction.
$\boldsymbol{A}, \boldsymbol{a}$	Matrix, vector.
$\boldsymbol{v}_s, \boldsymbol{i}_s, \boldsymbol{\psi}_s$	Stator voltage, current, and flux linkage.
$\boldsymbol{\psi}_M$	Stator flux linkage due to the magnet.
$\boldsymbol{\psi}_h$	Stator flux linkage with phase h.
$\boldsymbol{\psi}_{h,M}$	Stator flux linkage with phase h due to the magnet.
$\boldsymbol{i}_{se}$	Space vector of the equivalent flux current.
θ_r	Rotor (magnet) position.
$i_{h_+}/i_{h\_}$	Positive/negative peak current of phase h.
d-q/α-β	Rotor/stator fixed two-phase reference frames.
L_d, L_q	d-q synchronous inductances.
R	Phase resistance.
$\mu_s(\cdot)$	Membership function associated to the natural language value S.

Paper MSDAD-A 03–10, presented at the 2000 Industry Applications Society Annual Meeting, Rome, Italy, October 8–12, and approved for publication in the IEEE TRANSACTIONS ON INDUSTRY APPLICATIONS by the Industrial Automation and Control Committee of the IEEE Industry Applications Society. Manuscript submitted for review October 15, 2000 and released for publication August 22, 2003.

The authors are with the Department of Electrical Engineering, University of L'Aquila, 67040 L'Aquila, Italy (e-mail: tursini@ing.univaq.it; petrella@ing.univaq.it; rock@ing.univaq.it).

Digital Object Identifier 10.1109/TIA.2003.818977

I. INTRODUCTION

DEPENDING on the flux distribution or back-electromotive-force (EMF) waveform, permanent-magnet (PM) motors can be classified in two groups: the brushless dc motors (BLDCM) with trapezoidal back-EMF waveform and the synchronous motor (PMSM) with sinusoidal back-EMF.

The BLDCM is supplied by rectangular current pulses whose conduction duration is 120°. The commutation of each phase current is based on the rotor position information usually provided through devices which give an absolute information with 60° resolution (Hall sensors). This resolution is enough, at standstill, to assure the safe starting in the correct direction. BLDCM provides attractive features for a sensorless drive too, using back-EMF detection techniques. However, these methods do not give any information on the rotor position at standstill.

On the other hand, the PMSM is supplied with sinusoidal currents conveniently phased with respect to the corresponding back EMF. In this case a precise and continuous detection of the rotor position is required, achieved by position transducers such as encoders or resolvers. The use of cheap incremental encoders do not allow the knowledge of the initial position. Sensorless drives using rotor position estimation techniques are also available, but most of them do not detect the rotor position at standstill.

In the case of PM motors, the starting from an unknown rotor position may be accompanied by a temporary reverse rotation or may cause a starting failure. These eventualities are not tolerable in many applications [1]. Thus, when the initial rotor position information is not available, a proper starting procedure must be implemented for safe startup.

According to the various proposals in literature (a brief review can be found in [2]), the possible starting procedures can be grouped with reference to the basic principle as follows:

- starting from predetermined rotor position established by proper feeding;
- open-loop startup;
- estimation of the rotor position at standstill by means of specific algorithms.

The first method refers to the possibility of aligning the magnet axis in the direction of a (fixed) stator current field. This can be accomplished through closed loop current control (i.e., by the proper setting of the position feedback in a field oriented controller [3]), or in an open-loop scheme, simply imposing a specific inverter gate pattern to align with one of the phase axes [4]. The reliability of this method is affected by the presence of the load torque, whose value can cause a displacement between the imposed alignment position and the actual one.

The open loop startup is intended as the acceleration of the motor following a rotating stator field whose angular position is generated in an open-loop scheme.

This method is usually adopted in back-EMF-based sensorless scheme, and the open-loop operation is maintained until a given speed at which the rotor position estimate is sufficiently accurate [5]. The critical point of this method is the choice of the time-variation law of the open-loop position. It must be carefully selected in order to assure a safe starting with minimum oscillation up to the maximum torque [6].

Among the specific algorithms for rotor position estimation at standstill, an interesting approach is presented in [7] in the case of a field oriented scheme with incremental encoder. The rotor position is detected by considering the effect on the measured (incremental) position of a pseudorandom binary sequence test signal added to the direct current reference.

In regard to full sensorless applications, other methods must be applied. The most popular are based on the effect of the magnet position on the saturation of the stator flux paths (examples are given in [8]–[10], respectively, for a BLDCM and a PMSM). These methods employ proper current pulses as test signals. Despite of a certain time-to-set-up, they demonstrate an appreciable degree of robustness. Their precision relies both on the accuracy of the measurements and the exactness of the relations used for their processing, these last being often based on uncertain assumption on the system behavior.

In this paper, a method to detect the rotor position at standstill of PM motors is presented, based on the saturation principle. It is suitable to avoid temporary reverse rotation or starting failure. Particularly, it includes a fuzzy logic processing of the measured data capable to minimize the estimation error. The proposed method has been implemented on a last generation μC digital signal processor (DSP) (TMS320F240) suitable for electrical drive control systems. The obtained results confirm the effectiveness of the proposed solution. It is consistent with sensorless or nonabsolute position transducers based drives, with a wide range of motors (isotropic and nonisotropic, BLDCM and PMSM) and it does not require the knowledge of any of the motor parameters.

II. Basic Principle

The basic approach is the well-known method to estimate the rotor position by using the inductance variation due to the magnets position and an impressed stator current. A suitable sequence of voltage pulses is applied to the stator windings at standstill and the evaluation of the peak value of the current leads to the rotor position estimation. The principle can be explained with reference to the schematic PM motor shown in Fig. 1 as follows.

In the magnetic circuit of phase A, two effects are superimposed: the PM flux $(\psi_{A,M})$ and the phase current flux (ψ_A). If the phase current is positive (i_{A+}), the total flux linkage with the winding is

$$\psi_{A,\mathrm{tot}} = \psi_{A,M} + \psi_{A+}. \tag{1}$$

If the phase current is suitably high, the total flux saturates the magnetic circuit and the winding inductance is *low*.

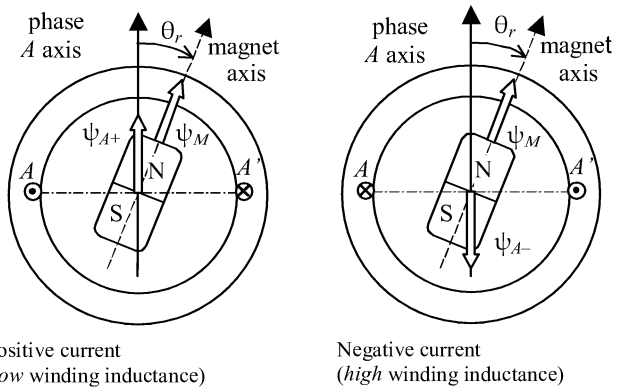

Fig. 1. Basic principle.

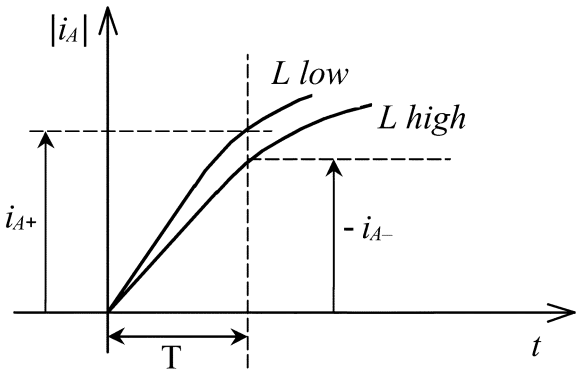

Fig. 2. Inductance variation due to saturation.

Now, if we change the sign of the current, the total flux becomes

$$\psi_{A,\mathrm{tot}} = \psi_{A,M} - \psi_{A-}. \tag{2}$$

In this case the magnetic circuit goes out of saturation and the winding inductance is *high*.

Actually, a positive voltage pulse V_{A+} is applied for a period T^+, then the phase current i_{A+} is measured and forced to zero. The procedure is repeated with a negative voltage pulse V_{A-} and the negative phase current i_{A-} is measured again (Fig. 2). If we compare the current amplitudes, we can define a *current difference*

$$\Delta i_A = i_{A+} + i_{A-}. \tag{3}$$

If this process is repeated for each phase, we obtain

$$\begin{aligned} \Delta i_A &= i_{A+} + i_{A-} \\ \Delta i_B &= i_{B+} + i_{B-} \\ \Delta i_C &= i_{C+} + i_{C-}. \end{aligned} \tag{4}$$

If the combination of the signs of the current differences is considered [8], it is possible to evaluate the rotor position with an accuracy of 60° (sector), which corresponds to the use of Hall sensors.

If we suppose that the values of the current differences vary continuously with the rotor position according to a certain law, the consideration of the inverse function allows to determine the

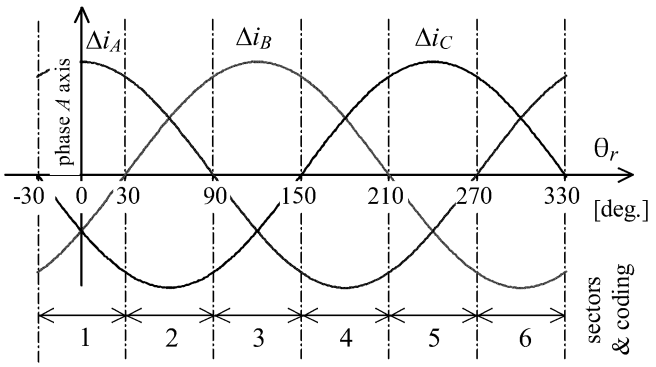

Fig. 3. Current differences for each phase (assumed sinusoidal) and position sectors.

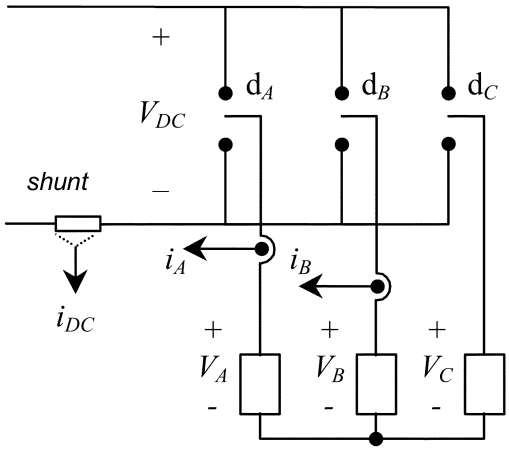

Fig. 4. Test scheme.

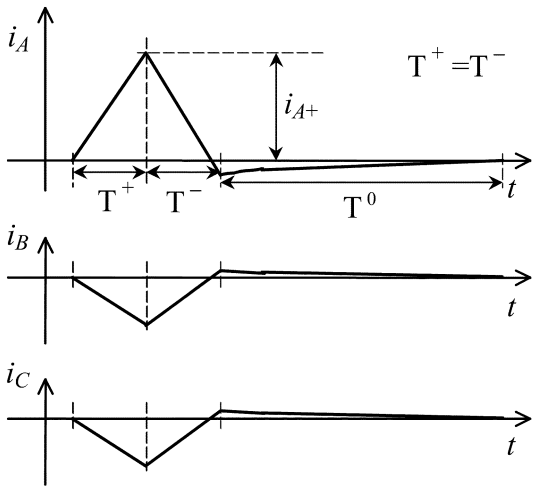

Fig. 5. Sequence for positive peak of current A.

TABLE I
FEEDING SEQUENCES

d_A d_B d_C	V_A/V_{DC}	V_B/V_{DC}	V_C/V_{DC}	i_{A+}	i_{A-}	i_{B+}	i_{B-}	i_{C+}	i_{C-}	i_{DC}	
– – –	0	0	0	T⁰	T⁰	T⁰	T⁰	T⁰	T⁰	0	0
+ – –	2/3	–1/3	–1/3	T⁺	T⁻					i_{A+}	V_{A+}
– + +	–2/3	1/3	1/3	T⁻	T⁺					$-i_{A-}$	V_{A-}
– + –	–1/3	2/3	–1/3			T⁺	T⁻			i_{B+}	V_{B+}
+ – +	1/3	–2/3	1/3			T⁻	T⁺			$-i_{B-}$	V_{B-}
– – +	–1/3	–1/3	2/3					T⁺	T⁻	i_{C+}	V_{C+}
+ + –	1/3	1/3	–2/3					T⁻	T⁺	$-i_{C-}$	V_{C-}
+ + +	0	0	0							0	

absolute rotor position. This kind of approach has been developed in [9] and [10], where a sinusoidal behavior of the current differences is assumed as shown in Fig. 3.

III. Basic Procedure

The implementation of this principle through a voltage-source inverter feeding is illustrated in Figs. 4 and 5 and Table I. Particularly, Fig. 5 shows the feeding sequence for the generation of the positive peak current of phase A. Starting with all the phase currents equal to zero, the positive voltage V_{A+} is obtained by closing the upper switch of the corresponding inverter leg, with the upper switches of the remaining legs opened. This pattern is applied for a time T^+, at the end of which the positive peak of current i_{A+} is sampled (due to the three phases feeding, in correspondence one has negative peaks for the other phase currents). Then, the complementary pattern V_{A-} is applied for a time $T^- = T^+$ in order to null the phase currents. Thereafter, the null voltage state is applied for a time T^0 long enough to have the freewheeling transients extinguished. A similar sequence is repeated to achieve the negative peak current i_{A-}, then the difference (3) is computed. The current differences for the other phases are obtained in a similar manner, the feeding voltage for each time period being reported in Table I.

In order to achieve a better understanding of the exposed phenomena, it has been analyzed by means of a simulation program which includes the basic procedure and the main system features such as the feeding inverter, control timing and digital sampling. Particularly, a PM synchronous motor model, which takes into account saturation phenomena, has been developed, as shown in the Appendix. Comparisons between simulation and experimental results are presented in the following.

The basic procedure has been tested by experiments using a μC DSP TMS320F240. Details on the hardware and software implementation are given in the Appendix, where the main data of the test motor are also listed.

Fig. 6 shows the measured current differences obtained using two Hall-effect-based current transducers for phases A and B (see Fig. 4). Actually, the measurements show significant uncertainties which affect the successive processing for rotor position detection (both as sector or absolute value).

- The current differences are not continuous and not sinusoidal; their processing to obtain the rotor position as suggested in [9] and [10] is critical.
- The signs of the differences are uncertain near the zero crossing, thus sector estimation is uncertain.
- Measurements are affected by offset errors, thus sector widths are different from 60°.

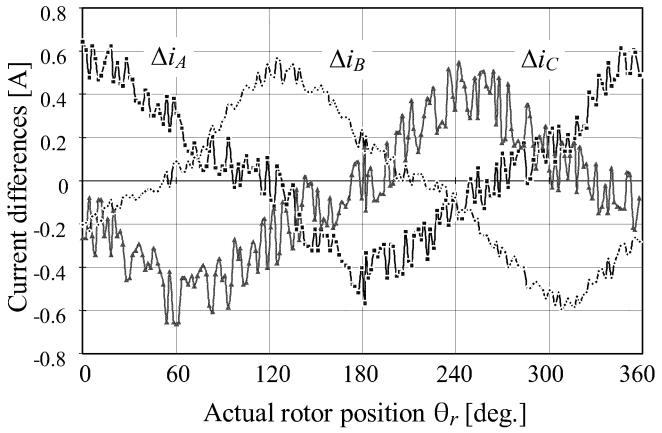

Fig. 6. Peak current differences (basic procedure).

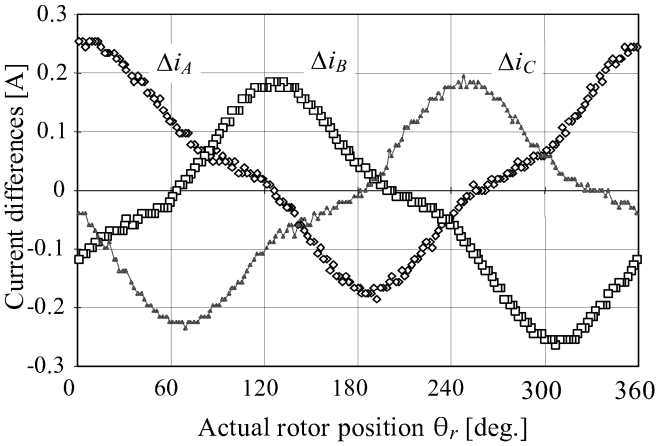

Fig. 7. Peak current differences (with average).

IV. Novel Detection Procedure and Experimental Results

In order to avoid these problems, the authors propose a novel procedure which combines an iteration of the pulses sequences with fuzzy logic processing of the current responses and phase currents derivation based on the dc-link current measurements. Particularly, the inclusion of fuzzy logic processing allows for enhancement of the accuracy of the estimated position being no longer limited to the 60° sector as in the basic procedure.

A. Iteration of the Pulses Sequences

Generation of positive and negative peak currents for each motor phase and calculation of current differences has been repeated a certain number of times in order to reduce the effects of measurement inaccuracy.

Fig. 7 shows the averages of the current differences obtained by imposing 16 current pulses (positive and negative) for each phase (the measurement system employs the two Hall-effect-based current transducers as for the results in Fig. 6). The shape of these functions is more continuous. As far as the sector calculation concerns, these profiles lead to certain sector evaluation, but the sector widths are still different due to offsets in the measuring circuitry, as shown in Fig. 8.

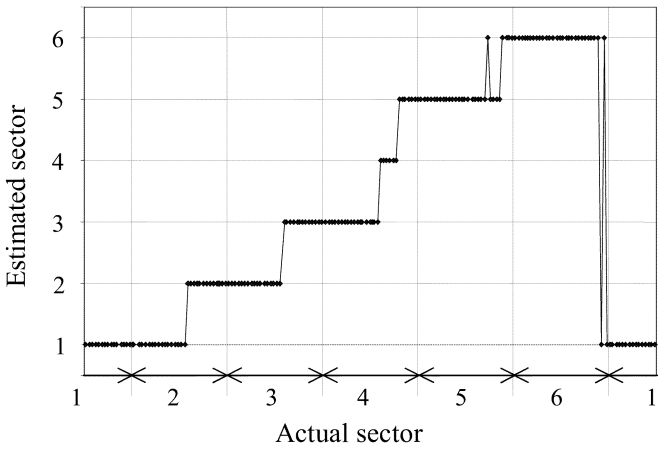

Fig. 8. Estimated versus actual position sector.

The implementation of the averaging process has simply been realized by repeating the basic estimation sequence a certain number of times. The mean value of the calculated current differences with respect to the number of programmed iterations is accumulated within each sequence leading directly to average current differences after the last cycle. Details on the software implementation are given in the Appendix.

B. Fuzzy Logic Processing

The presence of measurement uncertainties and the lack of a precise law of variation of the current differences suggest the use of a fuzzy logic processing to achieve a better approximation of the absolute rotor position.

The rotor position detection with fuzzy logic processing is implemented as follows.

1) According to fuzzy reasoning, in each sector a *positive* (or negative) current difference $\Delta i_{\mathrm{pos/neg}}$ is present which is big around the center of the sector and decreases toward the edges (see Fig. 3). The other two differences $\Delta i_{\mathrm{neg/pos,incr}}$ and $\Delta i_{\mathrm{neg/pos,decr}}$ are *negative* (or positive) medium around the center and respectively *increase* or *decrease* moving from one edge to the other. We first process those values in order to have a first current difference which is always positive and the other two negative (increasing and decreasing) as follows:

$$\begin{aligned}\Delta i_1 &= abs\left(\Delta i_{\mathrm{pos/neg}}\right)\\ \Delta i_2 &= \mathrm{sgn}\left(\Delta i_{\mathrm{pos/neg}}\right)\cdot \Delta i_{\mathrm{neg/pos,incr}}\\ \Delta i_3 &= \mathrm{sgn}\left(\Delta i_{\mathrm{pos/neg}}\right)\cdot \Delta i_{\mathrm{neg/pos,decr}}.\end{aligned}$$

2) The normalized values are then calculated by dividing for the maximum (absolute) value among them

$$\Delta i_{\max} = \max\left(\Delta i_1, |\Delta i_2|, |\Delta i_3|\right)$$
$$\Delta \hat{i}_1 = \frac{\Delta i_1}{\Delta i_{\max}} \quad \Delta \hat{i}_2 = \frac{\Delta i_2}{\Delta i_{\max}} \quad \Delta \hat{i}_3 = \frac{\Delta i_3}{\Delta i_{\max}}.$$

3) The sector is evaluated from the signs of the current differences, and the value of it center is set as default estimate of the rotor position $(\tilde{\vartheta}_r)$.

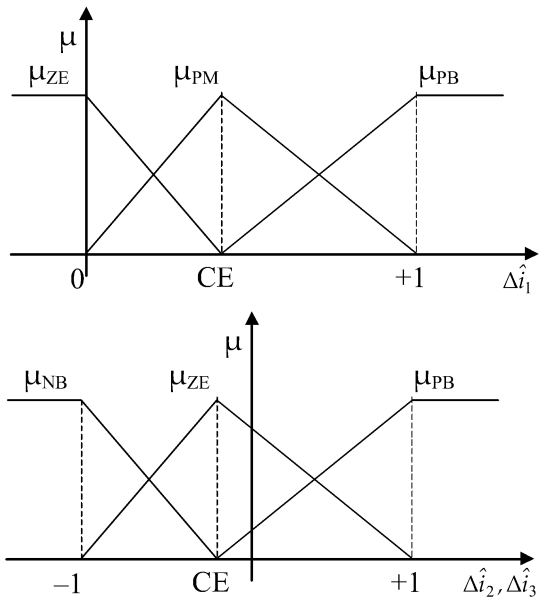

Fig. 9. Membership functions.

4) According with the signs and the expected shapes of the normalized current differences, two sets of natural language values are chosen to describe the values they can assume: ZE (zero), PM (positive medium), and PB (positive big) for $\Delta\hat{i}_1$, and NB (negative big), ZE (zero), and PB (positive big) for $\Delta\hat{i}_2$ and $\Delta\hat{i}_3$. These sets are grouped, respectively, as $S^{(p)} = \{ZE, PM, PB\}$ and $S^{(n)} = \{NB, ZE, PB\}$. Each element of the set will be indicated by $S_x^{(\cdot)}$ with $x = 1, 2, 3$. The choice to extend the universe of existence to positive values for $\Delta\hat{i}_2$ and $\Delta\hat{i}_3$ is related to the necessity to manage the measurement uncertainties near the zero crossing.
5) Then, fuzzy sets are associated to that natural language values and the corresponding (triangular) membership functions $\mu_{ZE}(\cdot)$, $\mu_{PM}(\cdot)$, $\mu_{PB}(\cdot)$ for $\Delta\hat{i}_1$, and $\mu_{NB}(\cdot)$, $\mu_{ZE}(\cdot)$, $\mu_{PB}(\cdot)$ for $\Delta\hat{i}_2$ and $\Delta\hat{i}_3$ are defined (Fig. 9).

   Parameter CE has been introduced to allow a certain degree of freedom when tuning the estimation algorithm during the development phase. Particularly it was experimented that its value affects the compensation for offsets in current measurement. It has been proven by experiments that both the number and the shape of the membership functions do not affect the reliability of the method nor the accuracy of the estimates. In fact, the more the number of the adopted membership functions increases, the more the "fuzzy" description of the current differences becomes "crisp," making the adoption of a fuzzy logic approach fruitless. Moreover, the method tends to become less robust to different shapes of current differences. In this sense, the adopted choice for three triangular membership functions has proved to be the best tradeoff among simplicity of implementation, execution times, accuracy of the estimates, and robustness.
6) Normalized current differences $\Delta\hat{i}_1$, $\Delta\hat{i}_2$, and $\Delta\hat{i}_3$ are inferred by the membership functions of Fig. 9. In the actual implementation the value of parameter CE has been fixed to -0.15 when inferring $\Delta\hat{i}_2$ or $\Delta\hat{i}_3$ and 0.5 when inferring $\Delta\hat{i}_1$.
7) The simplified method of Bernard is adopted for the defuzzification process. A set of 27 rules is defined as follows, each having three inputs (the current differences $\Delta\hat{i}_x$) and one output (defuzzified value $z_{i,j,k}$):

$$Rule_{i,j,k}(i = 1,2,3, j = 1,2,3, k = 1,2,3):$$
$$\textbf{if } \left[\left(\Delta i_1 \text{ is } S_i^{(p)}\right) \text{ and } \left(\Delta i_2 \text{ is } S_j^{(n)}\right) \text{ and } \left(\Delta i_3 \text{ is } S_k^{(n)}\right)\right]$$
$$\textbf{then } (z_{i,j,k} = \textbf{CORR}_{i,j,k})$$

   $z_{i,j,k}$ being the simple correction action produced by $Rule_{i,j,k}$ to the default estimate $\tilde{\vartheta}_r$ of the rotor position and **CORR** a $3 \times 3 \times 3$ matrix of correction values.

   In the actual implementation, the correcting action can be either positive or negative and it is expressed as a fraction of 60 electrical degrees. This choice has proven to increase the precision of estimation at the edges of the sector. The matrix **CORR** of the correction values is

$$CORR_{ZE,j,k} = \begin{bmatrix} 0 & -0.3 & -0.6 \\ 0.3 & 0 & -0.3 \\ 0.6 & 0.3 & 0 \end{bmatrix} \quad \left(\Delta\hat{i}_1 \; is \; ZE\right)$$
$$CORR_{PM,j,k} = \begin{bmatrix} 0 & -0.6 & -0.9 \\ 0.6 & 0 & -0.6 \\ 0.9 & 0.6 & 0 \end{bmatrix} \quad \left(\Delta\hat{i}_1 \; is \; PM\right)$$
$$CORR_{PB,j,k} = \begin{bmatrix} 0 & -0.5 & -1 \\ 0.5 & 0 & -0.5 \\ 1 & 0.5 & 0 \end{bmatrix} \quad \left(\Delta\hat{i}_1 \; is \; PB\right).$$

8) The degree of fulfilment (DOF) of $Rule_{i,j,k}$ is defined as follows:

$$DOF_{i,j,k} = \min\left[\mu_{S_i^{(p)}}(\Delta\hat{i}_1), \mu_{S_j^{(n)}}(\Delta\hat{i}_2), \mu_{S_k^{(n)}}(\Delta\hat{i}_3)\right].$$

9) The inferred value from $Rule_{i,j,k}$ is the output of that rule weighted by its degree of fulfilment, that is,

$$DOF_{h,j,k} \cdot z_{h,j,k}.$$

10) The final value of the correction to the default estimate $\tilde{\vartheta}_r$ of the rotor position is obtained by the weighted mean value of the simple correction actions $z_{i,j,k}$, that is,

$$\Delta\tilde{\vartheta}_r = \frac{\sum_{i,j,k} DOF_{i,j,k} \cdot z_{i,j,k}}{\sum_{h,j,k} DOF_{i,j,k}} \text{(Center of Gravity Method)}.$$

11) Finally, the absolute rotor position is obtained as $\tilde{\vartheta}_r + 60 \cdot \Delta\tilde{\vartheta}_r$.

The fuzzy logic processing has been implemented in assembly language by using 16-bit fixed-point numerical representation. Calculation of the membership functions and DOFs have been implemented by means of dedicated and time-optimized functions which are recalled by the main fuzzy processing algorithm. The resulting execution time is about 22 μs (worst case).

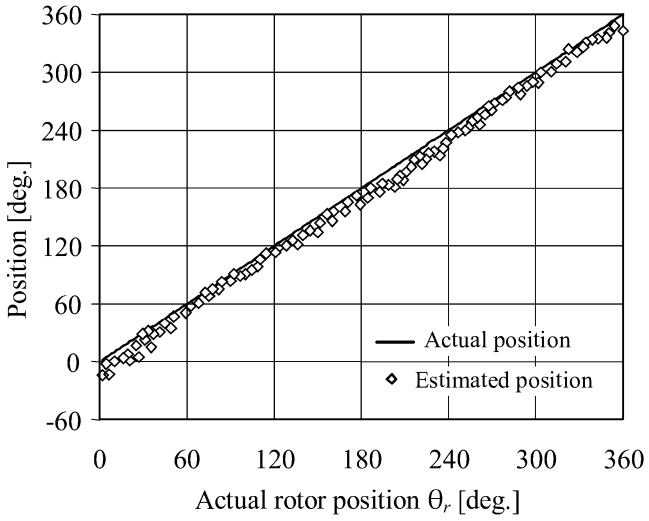

Fig. 10. Estimated versus actual position.

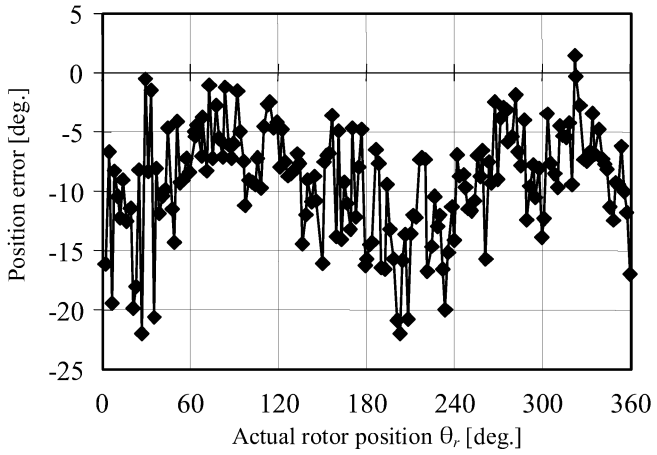

Fig. 11. Position estimation error.

Figs. 10 and 11 show the comparison between the actual and the estimated rotor position by using the proposed fuzzy logic processing. The position error is consistent with BLDCM starting procedure (sector information) as well PMSM starting procedure (absolute rotor position).

C. DC-Link Current Measurement

Further improvement at the measurement level has been obtained using phase currents derivation based on the dc-link current measurements.

Let us suppose to use the classical Hall-effect transducers on each motor phase to obtain current samples $i_{h+,\mathrm{SAMPLE}}$ and $i_{h-,\mathrm{SAMPLE}}$, with $h \in \{A, B, C\}$.

If gain and offset errors are taken into account in the measuring process, current samples differ from actual currents, that is,

$$\begin{aligned} i_{h+,\mathrm{SAMPLE}} &= k_h \cdot i_{h+} + i_{h,\mathrm{offset}} \\ i_{h-,\mathrm{SAMPLE}} &= k_h \cdot i_{h-} + i_{h,\mathrm{offset}} \end{aligned} \tag{5}$$

where $k_h > 0$ and $i_{h,\mathrm{offset}}$ are, respectively, the gain and the offset errors for the measuring circuitry of phase h. If we compute the current difference $\Delta i_{h,\mathrm{SAMPLE}}$, we obtain

$$\begin{aligned} \Delta i_{h,\mathrm{SAMPLE}} &= i_{h+,\mathrm{SAMPLE}} + i_{h-,\mathrm{SAMPLE}} \\ &= k_h \cdot (i_{h+} + i_{h-}) + 2 \cdot i_{h,\mathrm{offset}} \\ &= k_h \cdot \Delta i_h + 2 \cdot i_{h,\mathrm{offset}}. \end{aligned} \tag{6}$$

As the basic estimation method presented in Sections IV-A and B is based on the evaluation of the sign of current differences disregarding of their amplitude, thus gain errors have no influence. On the other hand, the offset errors are of great importance and could lead to wrong sector evaluation. Even in the case of fuzzy processing of current differences, gain errors have no influence as normalization of those differences is considered but, also in this case, offset errors lead to wrong sector evaluation that could not be compensated by fuzzy logic processing.

In order to overcome these problems, the authors propose a simple but efficient method to obtain current samples which uses only one shunt resistor on the lower dc bus of the inverter (see Fig. 4). This method allows us to obtain the required current differences with the same gain errors and no offset errors.

The principle of the phase currents derivation based on the dc-link current measurements is well known [11], [12]: for each of the six active states of the inverter, the dc-link current is exactly equal to one of the phase currents or its opposite, while during the two zero states the dc-link current is zero since all motor currents are freewheeling.

According to Table I, the following current samples are obtained:

$$\begin{aligned} i_{h+,\mathrm{SAMPLE}} &= k \cdot i_{h+} + i_{\mathrm{offset}} \\ i_{h-,\mathrm{SAMPLE}} &= k \cdot (-i_{h-}) + i_{\mathrm{offset}} \end{aligned} \tag{7}$$

where $k > 0$ and i_{offset} are, respectively, the gain and the offset errors for the measuring circuitry in the dc link. If we compute the current difference $\Delta i_{h,\mathrm{SAMPLE}}$, we obtain

$$\begin{aligned} \Delta i_{h,\mathrm{SAMPLE}} &= i_{h+,\mathrm{SAMPLE}} - i_{h-,\mathrm{SAMPLE}} \\ &= k \cdot (i_{h+} + i_{h-}) = k \cdot \Delta i_h. \end{aligned} \tag{8}$$

Thus, the accuracy of the calculation of the current differences is not affected anymore by the offset that could be present in the measuring circuitry. Moreover, the gain error is the same for all the current differences.

The reliability of current sampling also depends on the correct synchronizing of the A/D conversion module operation with the pulsewidth-modulation (PWM) pattern. In fact, as shown in Fig. 12, by considering that the sample-and-hold circuitry takes about 1 μs to acquire the dc-link current sample, the sampling instant should be properly anticipated with respect to the PWM pattern modification in order not to sample the commutation transient.

In the actual implementation by using the TMS320F240 this can be achieved without recourse to any external hardware. In fact, referring to Fig. 13, the A/D start of conversion (SOC) signal can be provided by the compare logic associated to the

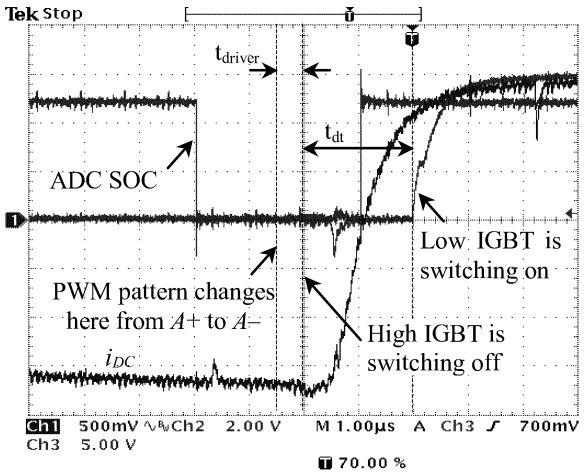

Fig. 12. Sampling of the dc current.

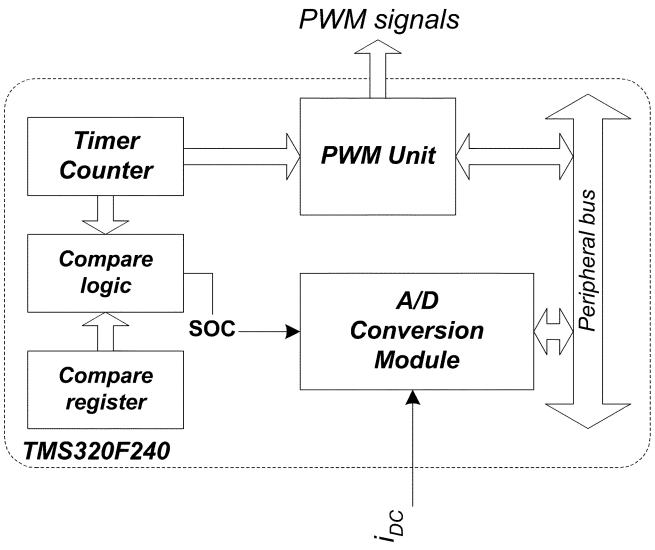

Fig. 13. μC DSP subsystems used to synchronize current sampling.

same timer used to generate PWM signals. Then, the sampling instant can be easily defined and synchronized with respect to the PWM pattern.

Figs. 14–16 show the current differences, the estimation errors, and the comparison between the actual and the estimated rotor position by using the dc-link current measurement. Fig. 17 shows the amplitude of the positive peak current with respect to the rotor position. The comparison with simulations (Figs. 14 and 17) shows a good agreement and confirms the effectiveness of the proposed procedure. Finally, Fig. 18 presents the comparison between the proposed method (*estimation*) and the starting procedure which imposes a predetermined position established by specific impressed currents (*initialization*). The position errors (with respect to the actual position for the "estimation", and to the predetermined position for the "initialization") are shown as a function of the load (braking) torque at standstill. Several tests are reported for each load with different (random) initial actual rotor position. In the case of the initialization method the errors are heavily affected by the load, while the proposed estimation method does not depend on it.

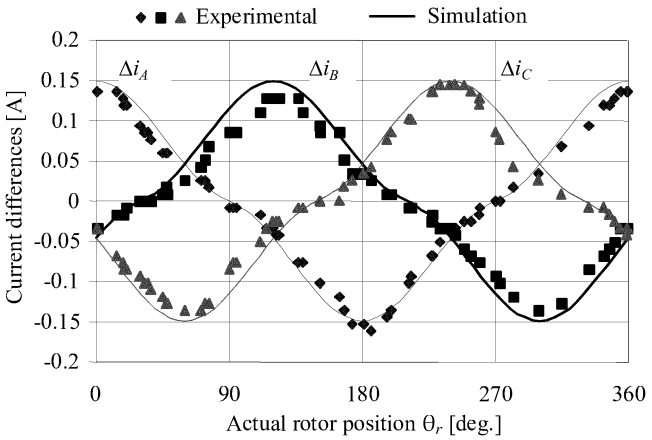

Fig. 14. Peak current difference (dc-link measurement).

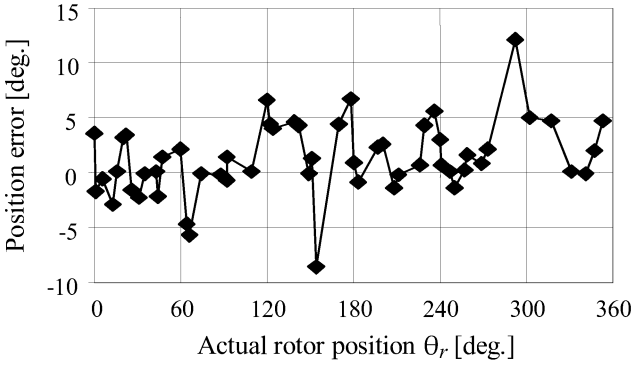

Fig. 15. Position estimation error (dc-link measurement).

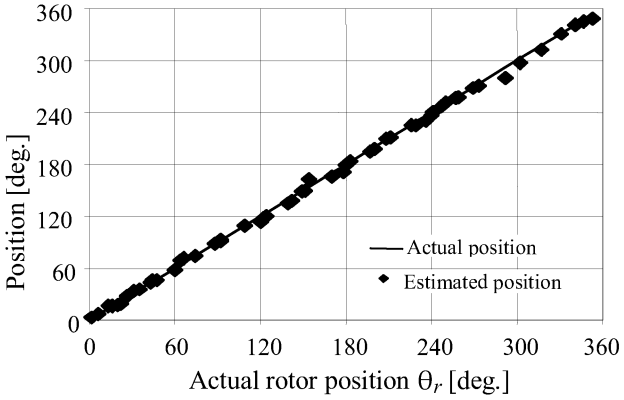

Fig. 16. Estimated versus actual position (dc-link measurement).

V. Conclusion

In this paper, a novel solution to detect the rotor position at standstill of PM motors is proposed. It is based on the investigation of the stator inductance variation as a function of the rotor magnets position and the stator current space vector. The procedure combines an iterative sequence of voltage pulses with fuzzy logic processing of the current responses and phase currents derivation based on the dc-link current measurements.

It can be applied with a wide range of motors (isotropic and nonisotropic, BLDCM, and PMSM) and it does not require the knowledge of any of the motor parameters.

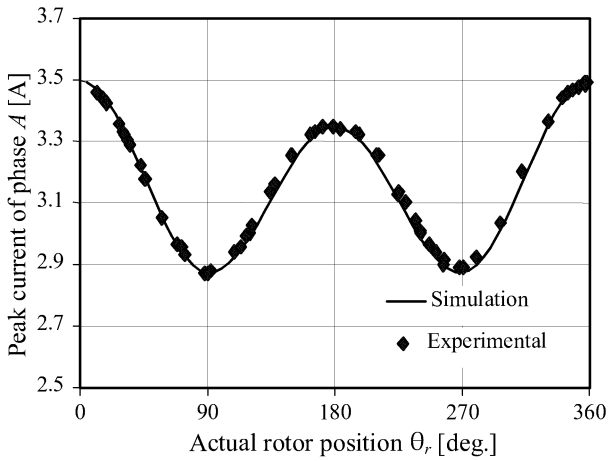

Fig. 17. Positive peak current of phase A.

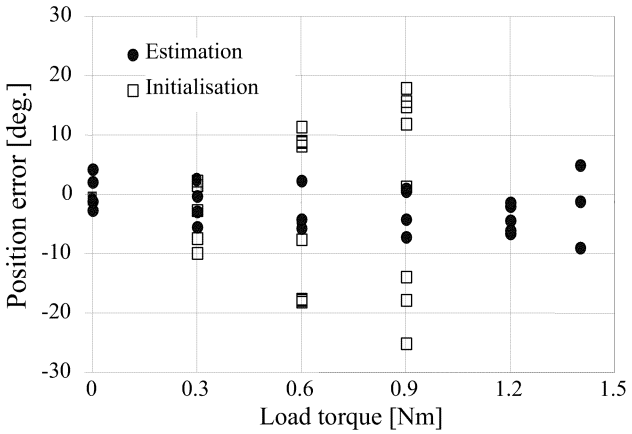

Fig. 18. Position error by different methods.

In sensorless drives, it could be used in combination with an open-loop starting procedure and algorithms not able to estimate the rotor position at standstill.

In case of drives which are equipped with nonabsolute position transducers, the use of the proposed method allows to remove the conventional starting procedure that could imply small rotations which are not desired or not possible at standstill.

APPENDIX

A. PM Motor Model With Saturation

As known, if the stator windings are sinusoidally distributed in space, the phenomena of saturation of the flux paths can be represented by using the space vector or two-axis theory, with a remarkable gain in easiness of exposition and comprehension.

Assuming, for the matter of generality, a magnetically salient PMSM, the electrical equations in terms of stator fixed-axis components $\alpha\beta$ are (the meaning of the symbols used are clarified in the nomenclature)

$$\begin{aligned} \boldsymbol{v}_s &= R\boldsymbol{i}_s + \frac{d\boldsymbol{\psi}_s}{dt} \\ \boldsymbol{\psi}_s &= \boldsymbol{L}_s(\vartheta_r)\,\boldsymbol{i}_s + \boldsymbol{\psi}_M(\vartheta_r) \end{aligned} \tag{9}$$

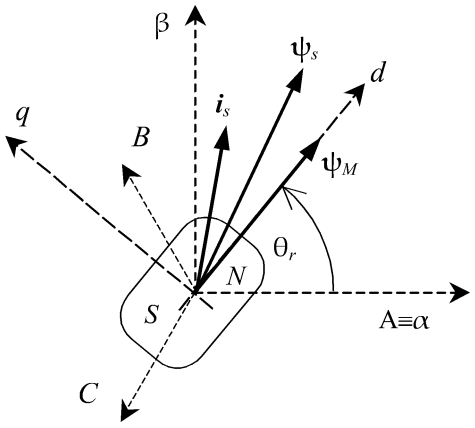

Fig. 19. Flux and current space vectors in a PM synchronous motor.

where the space vector of the flux linkage due to the magnet is given by

$$\boldsymbol{\psi}_M = \hat{\psi}_M \begin{bmatrix} \cos\vartheta_r \\ \sin\vartheta_r \end{bmatrix} \tag{10}$$

and the matrix of the winding inductance is

$$\boldsymbol{L}_s = \begin{bmatrix} L_\alpha & L_{\alpha\beta} \\ L_{\alpha\beta} & L_\beta \end{bmatrix} \tag{11}$$

with

$$\begin{aligned} L_\alpha &= \frac{L_d + L_q}{2} + \frac{L_d - L_q}{2}\cos(2\vartheta_r) \\ L_\beta &= \frac{L_d + L_q}{2} - \frac{L_d - L_q}{2}\cos(2\vartheta_r) \\ L_{\alpha\beta} &= \frac{L_d - L_q}{2}\sin(2\vartheta_r) \end{aligned} \tag{12}$$

L_d and L_q being the *direct* and *quadrature* synchronous inductances, respectively, which in the case of saturation vary as a function of the flux (i.e., current) level.

Extending the approach followed in [13] for wound field to PM synchronous machines, the effect of saturation can be taken into account in terms of an equivalent flux current as follows.

Let us consider the stator flux linkage expressed in terms of rotor fixed-axis components d-q (Fig. 19)

$$\begin{aligned} \psi_d &= L_d i_d + \hat{\psi}_M \\ \psi_q &= L_q i_q. \end{aligned} \tag{13}$$

The contribution of the magnet to the stator flux linkage can be expressed in terms of an equivalent "magnet" current acting along the d axis as

$$\hat{i}_M = \frac{\hat{\psi}_M}{L_d}. \tag{14}$$

By the comparison of (13) and (14) an equivalent space vector $\boldsymbol{i}_{se}$ responsible for the whole stator flux linkage can be defined as follows (Fig. 20):

$$\begin{aligned} i_{de} &= i_d + \hat{i}_M \\ i_{qe} &= i_q. \end{aligned} \tag{15}$$

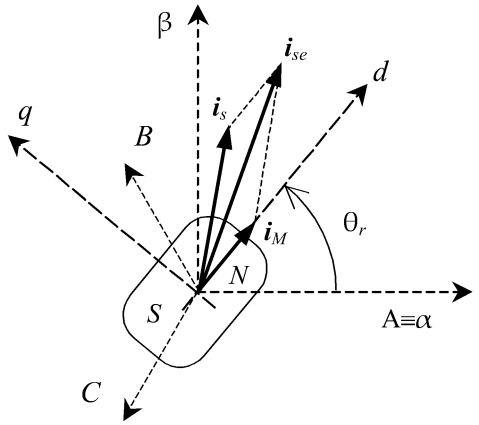

Fig. 20. Stator flux linkage equivalent current.

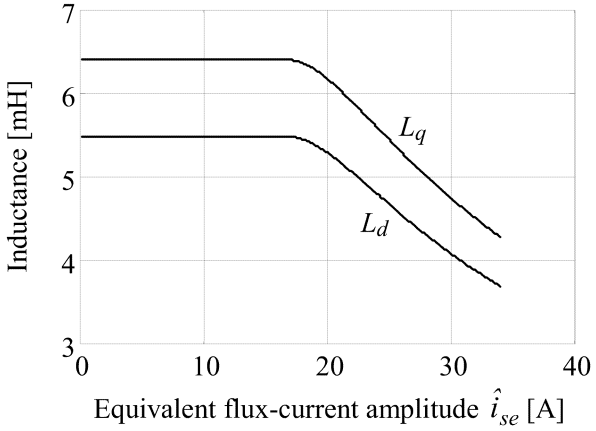

Fig. 21. Synchronous inductances profiles.

Assuming that in each axis the saturation level is determined by the amplitude of the space vector of the equivalent stator current

$$\hat{i}_{se} = \sqrt{i_{de}^2 + i_{qe}^2} \tag{16}$$

the synchronous inductances accounting for saturation are

$$L_d(\hat{i}_{se}) \quad L_q(\hat{i}_{se}) \tag{17}$$

and the stator flux linkages can be written as

$$\begin{aligned} \psi_d &= L_d(\hat{i}_{se}) \cdot i_{de} \\ \psi_q &= L_q(\hat{i}_{se}) \cdot i_{qe}. \end{aligned} \tag{18}$$

As is clear from Fig. 20, the angle between the stator current and the magnet axis affects the amplitude of the equivalent current, i.e., the saturation level. Thus, the use of the synchronous inductances curves (17) in the model (9)–(12) allows us to simulate the PMSM behavior in saturation conditions. Fig. 21 shows the inductance profiles of the test machine considered in the paper.

B. DSP Implementation

This section presents the implementation of the presented rotor position estimation technique using the μC DSP TMS320F240.

The temporization diagram of a slice of the estimation sequence is presented in Fig. 22. The estimation algorithm is hosted inside the control routine. Each control period is synchronized with the PWM period (T_{PWM}), at the beginning of which current sampling (which takes about 6 μs) is performed and the estimation sequence handling code is executed. The estimation sequence is executed once at the startup of the drive or it can be repeated when the drive is disabled (for testing and debugging purposes).

Fig. 23 shows the simplified flowchart of the estimation algorithm which implements the "basic procedure" described in Section III.

The main steps which are performed are:

- check whether the estimation sequence is over or not;
  - if yes, calculate the estimated sector and disable the estimation algorithm;
  - if not:
    - retrieve the PWM pattern that will be applied during the next modulation period ("*New estimation pattern*") together with the number of modulation periods that pattern will be applied for ("*EstimationStep*"). In fact, as discussed in Section III, each active pattern (either positive or negative voltage pulses) is applied for a sufficient time to allow the current to grow up till a value which produces the saturation of the magnetic circuit, this time being a function of the motor parameters. Thus, in the actual implementation, each active pattern is only applied once, while the modulation period is defined (only for the estimation procedure) according to the adopted motor. In practical cases, when considering small-power motors (some hundreds of watts), the application time for each active pattern (V_{A+}, V_{A-}, etc.) is in the range 40–200 μs, depending on the phase inductance value.
    - check whether to save or discard available current samples (depending on previous PWM pattern); in fact, as current sampling is executed every period on the underflow of the PWM carrier, one flag ("*StoreCurrentsFlag*") has been introduced meaning that the last current samples are valid for estimation processing;
    - calculate current difference (only if two current samples are already available).

The time length of the basic estimation sequence depends on motor characteristics, which define times T^+, T^-, and T^0 as stated before. In practical cases, a time of about 10 ms can be reasonable. The execution time of the estimation algorithm is about 5μs (at 20-MHz clock frequency) in the worst case.

Fig. 24 shows the flowchart of the modified estimation algorithm which implements the "novel procedure" described in Section IV.

The differences from the previous one are highlighted (in boldface) and regard:

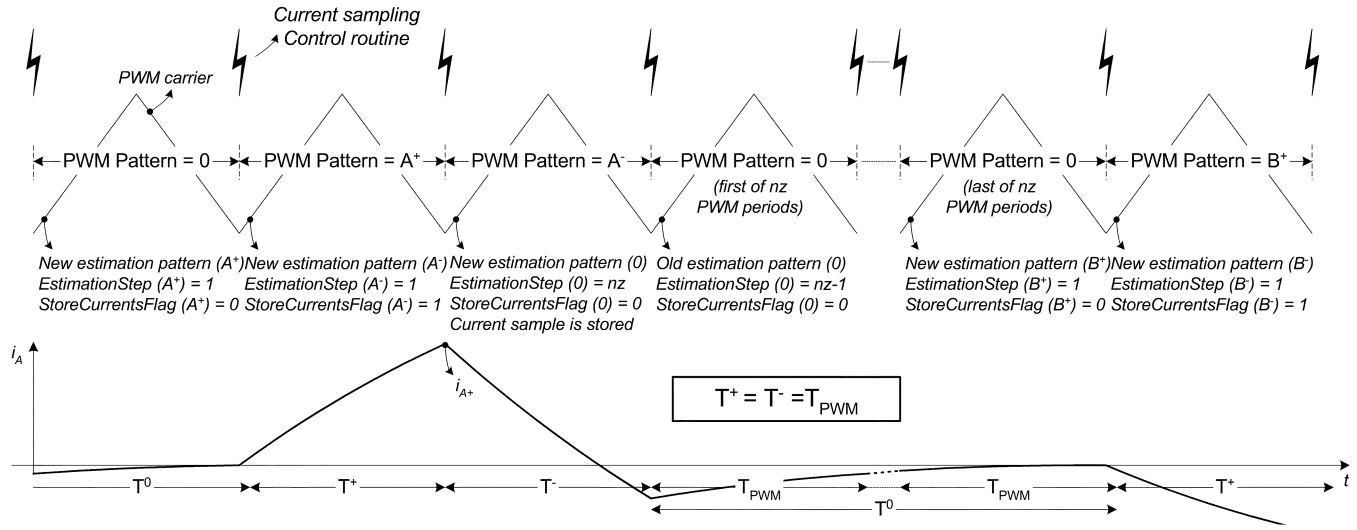

Fig. 22. Example of an estimation pattern and corresponding phase current behavior.

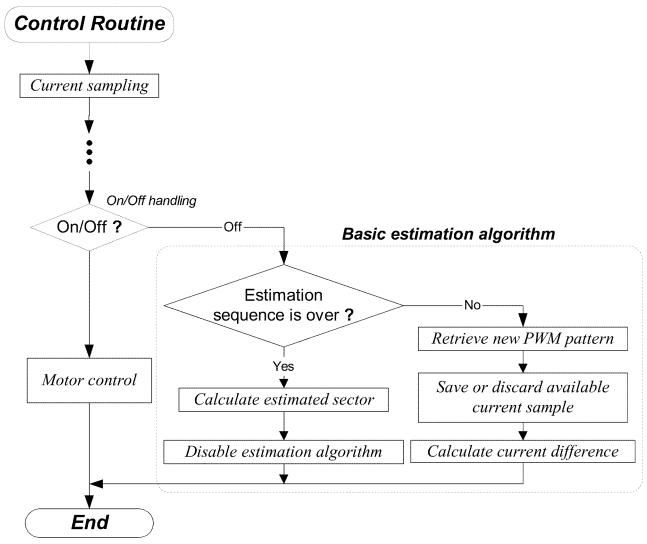

Fig. 23. Flowchart of the basic estimation procedure.

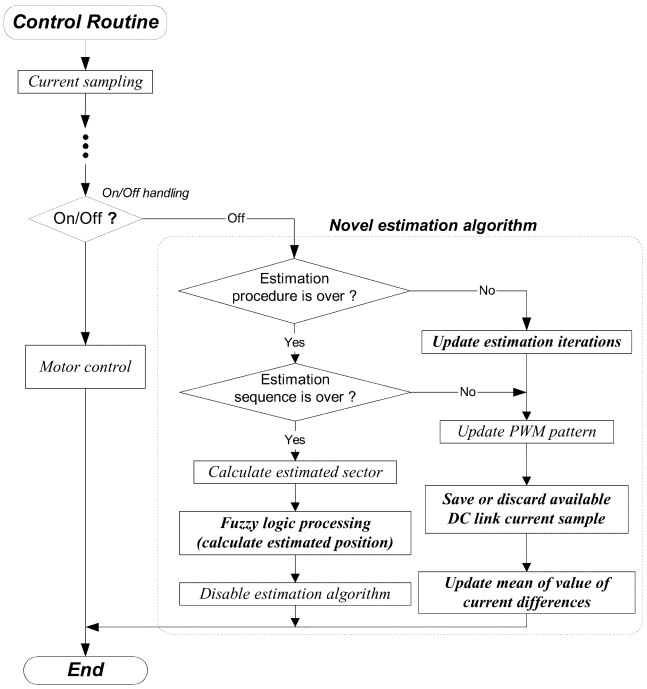

Fig. 24. Flowchart of the novel estimation procedure.

- the handling of multiple estimation sequences for averaging purposes;
- the introduction of a fuzzy logic algorithm for the processing of the average values of current differences;
- the handling of the dc-link current sample for the reconstruction of the motor phase current.

With respect to the basic procedure, the execution time of the estimation algorithm increases to 27 μs, due to the presence of fuzzy logic processing.

The possibility of adopting the presented implementation with a given range of motors depends on the value of $T^+ = T_{\rm PWM}$, and is then somewhat limited by the processing performance of the microcontroller, as the time needed for the algorithm execution must stay within $T_{\rm PWM}$. Nevertheless, only the execution time of the basic estimation algorithm plus current sampling and interrupt latency (that is about 12 μs) should be considered, as the fuzzy processing is actually a simple post-processing of the current differences. Therefore, different implementation could be proposed to overcome that limitation, as the estimation methodology itself has no real-time requirements and virtually do not introduce any constraint on the microcontroller processing speed.

C. Test Motor

The experiments described in this paper were carried out using the following PMSM:

pole pairs	4;
rated voltage (peak)	254 V;
rated current (peak)	3.53 A;
rated (base) speed	3000 r/min;
rated torque	2 N·m;
R	1.9 Ω;
L_d, L_q	see Fig. 21.

REFERENCES

[1] G. Pfaff, A. Weschta, and A. Wick, "Design and experimental results of a brushless AC servo drive," *IEEE Trans. Ind. Applicat.*, vol. 20, pp. 814–821, July/Aug. 1984.

[2] N. Matsui, "Sensorless PM brushless DC motor drives," *IEEE Trans. Ind. Electron.*, vol. 43, pp. 300–308, Apr. 1996.

[3] F. Parasiliti and M. Tursini, "Study and simulation of a permanent magnet synchronous motor drive," *L'Energia Elettrica*, no. 12, pp. 621–634, Dec. 1989.

[4] N. Matsui, "Sensorless operation of brushless DC motor drives," in *Proc. IEEE IECON'93*, 1993, pp. 739–744.

[5] F. Parasiliti, R. Petrella, and M. Tursini, "Sensorless speed control of a PM synchronous motor by sliding mode observer," in *Proc. IEEE ISIE'97*, Guimarães, Portugal, 1997, pp. 1106–1111.

[6] ——, "Rotor speed and position detection for PM synchronous motors based on sliding mode observer and kalman filter," in *Conf. Rec. EPE Conf.*, Lausanne, Switzerland, 1999, CD-ROM.

[7] B. Orlik, "Methods of parameter determination to detect the pole position of synchronous motors with permanent magnet excitation using incremental shaft encoders," in *Proc. EPE Conf.*, Aachen, Germany, 1989, pp. 1213–1218.

[8] L. Cardoletti, A. Cassat, and M. Jufer, "Indirect position detection at standstill for brushless DC and step motors," in *Proc. EPE Conf.*, Aachen, Germany, 1989, pp. 1219–1222.

[9] N. Matsui, "Sensorless permanent-magnet brushless DC and synchronous motor drives," in *Proc. Electromotion 3*, 1996, pp. 172–180.

[10] P. B. Schmidt, M. L. Gasperi, G. Ray, and A. H. Wijenayake, "Initial rotor angle detection of nonsalient pole permanent magnet synchronous machine," in *Conf. Rec. IEEE-IAS Annu. Meeting*, New Orleans, LA, 1997, pp. 459–463.

[11] F. Blaabjerg, J. K. Pedersen, U. Jaeger, and P. Thoegersen, "Single current sensor technique in the DC link of three-phase PWM-VS inverters: A review and a novel solution," *IEEE Trans. Ind. Applicat.*, vol. 33, pp. 1241–1253, Sept./Oct. 1997.

[12] F. Parasiliti, R. Petrella, and M. Tursini, "Low cost phase current sensing in DSP based AC drives," in *Proc. IEEE ISIE'99*, Bled, Slovenia, 1999, pp. 1284–1289.

[13] P. Vas, *Electrical Machines and Drives: A Space-Vector Theory Approach*. London, U.K.: Oxford Univ. Press, 1992.

Marco Tursini (M'99) was born in S.Pio delle Camere, Italy, in 1960. He received the M.S. degree in electrical engineering from the University of L'Aquila, L'Aquila, Italy, in 1987.

In 1987, he joined the Department of Electrical Engineering, University of L'Aquila, as an Associate Researcher. He became an Assistant Professor of power converters, electrical machines, and drives in 1991, and an Associate Professor of electrical machines in 2002. In 1990, he was a Research Fellow in the Industrial Electronics Laboratory, Swiss Federal Institute of Technology, Lausanne, Switzerland, where he conducted research on sliding-mode control of permanent-magnet synchronous motor drives. His research interests are focused on advanced control of ac drives, including vector, sensorless, and fuzzy logic control, digital motion control, DSP-based systems for real-time implementation, and modeling and simulation of electrical drives. He has authored more than 70 technical papers on these subjects.

Roberto Petrella (S'99–M'00) was born in Pescara, Italy, in 1971. He received the M.S. degree in electronic engineering, with honors, and the Ph.D. degree from the University of L'Aquila, L'Aquila, Italy, in 1996 and 2001, respectively.

During his M.S. studies, he received praise from the evaluating commission for the excellent results obtained in the development of a research and industrial project. In 1997, he joined the Department of Electrical Engineering, University of L'Aquila, as a Research Fellow. He is currently a Post-Doctoral Fellow in the same department. His main research interests include advanced control of electrical drives (including vector control, energy efficiency optimization techniques, estimation techniques, and sensorless control), digital motion control, and high-performance DSP-based systems for real-time control. He has authored more than 30 technical papers on these topics.

Francesco Parasiliti was born in Tortorici, Italy, in 1956. He received the M.S. degree in electrical engineering from the University of Rome, Rome, Italy, in 1981.

In 1983, he joined the Department of Electrical Engineering, University of L'Aquila, L'Aquila, Italy, as an Assistant Professor. He became an Associate Professor of electrical drives in 1992, and a Full Professor in 2000. From 1987 to 1988, he was a Research Fellow at the Swiss Federal Institute of Technology, Lausanne, Switzerland. His studies deal with design optimization of induction, permanent-magnet synchronous, and reluctance motors, modeling and parameter observation of induction and synchronous machines, and digital control of electrical drives including vector, sensorless, and fuzzy logic control.